Ibrahim Ahmed B.M. (Orcid ID: 0000-0003-4748-6135)
Mahmoud Ghada Abd-Elmonsef (Orcid ID: 0000-0002-4760-9871)
Cordes David B. (Orcid ID: 0000-0002-5366-9168)
Slawin Alexandra M. Z. (Orcid ID: 0000-0002-9527-6418)

Pb(II) and Hg(II) Thiosemicarbazones for Inhibiting the Broad-Spectrum Pathogen *Cladosporium sphaerospermum* ASU18 (MK387875) and Altering Its Antioxidant System

Short title: Effect of metal thiosemicarbazones on fungus antioxidant system

Ahmed B.M. Ibrahim,[a] Ghada Abd-Elmonsef Mahmoud,[b] David B. Cordes,[c] Alexandra M. Z. Slawin[c]*

[a]Department of Chemistry, Faculty of Science, Assiut University, Assiut 71516, Egypt

[b]Department of Botany & Microbiology, Faculty of Science, Assiut University, Assiut 71516, Egypt

[c]EaStCHEM School of Chemistry, University of St Andrews, Fife, KY16 9ST, U.K.

**Corresponding author: E-mail: aibrahim@aun.edu.eg*

Orcid (Ibrahim): https://orcid.org/0000-0003-4748-6135

Orcid (Mahmoud): https://orcid.org/0000-0002-4760-9871

ORCID (Cordes): https://orcid.org/0000-0002-5366-9168

ORCID (Slawin): https://orcid.org/0000-0002-9527-6418

This article has been accepted for publication and undergone full peer review but has not been through the copyediting, typesetting, pagination and proofreading process which may lead to differences between this version and the Version of Record. Please cite this article as doi: 10.1002/aoc.6798

Abstract

Pb(II) and Hg(II) ions were reacted in aqueous solution with two tridentate thiosemicarbazones, resulting in four complexes {[Pb(L^1)$_2$] **1**, [Pb(L^2)$_2$] **2**, [Hg(L^1)$_2$] **3** and [Hg(L^2)$_2$] **4**; **HL^1** = 4-(4-nitrophenyl)-1-((pyridin-2-yl)methylene)thiosemicarbazide and **HL^2** = 4-(2-chlorophenyl)-1-((pyridin-2-yl)methylene)thiosemicarbazide}. The solid-state structures of complexes **2** and **3** were determined by X-ray crystallography, which also confirmed the monobasic tridentate NNS nature of the ligands, and the octahedral coordination geometry around the metal centers. Complexes **1-4** exhibited high antifungal activity against the pathogen *Cladosporium sphaerospermum*; all four complexes giving rise to a reduction in the fungal dry mass and sugar consumption. Complexes **2** and **4** that inhibited *Cladosporium sphaerospermum* growth at the concentration of 1.8 mM are more efficient inhibitors than the free ligand and metal ions. Further, the complexes gave varied values of the fungal total antioxidants (TA), superoxide dismutase (SOD) and catalase (CAT) activities dependent on their concentrations.

Keywords: NNS ligands; Heavy metals; Pathogen; Catalase; Superoxide dismutase.

1. Introduction

The medicinal applicability of the thiosemicarbazones (TSCs) and their respective metal complexes as antimicrobial, antiviral, antimalarial and antitumor drugs [1-5] has urged various research groups worldwide to further investigate these complexes [6-9]. TSCs are versatile ligands capable of affording a variety of coordination modes in neutral and in monoanionic forms [7,10] and their biological behavior has documented to depend on the substitution at N-4 position [6]. The compounds in the pyridine-2-carboxaldehyde thiosemicarbazones are tridentate NNS ligands that lead to metal complexes with chelation-enhanced stability and enhanced biological applicability via synergy with metal cations [11].

Microbes can survive at heavy metal stress concentration up to a certain level beyond this concentration disruption in the cell defense enzymes and the entire cell physiology usually occurs [12]. Indeed, heavy metals affect the overall essential metal ion content and can change the cell membrane permeability, the growth rate and the morphology of the microorganisms causing reduction in both hyphal extension and microbial biomass as well as abnormality in mycelia [13]. This is in addition to the metal ability, at certain concentrations, to influence the cell ATP and ADP content [14]. Lead and mercury compounds are regarded as bio-accumulative and hazardous compounds for cells [15], as they specifically interact with the nucleic DNA and RNA acids and with the cellular sulfur and nitrogen containing amino acid ligands disrupting many metabolic pathways [12,16]. Flora et. al. [17] reported the relationship between the cell exposure to heavy metals and the formation of reactive oxygen species which produce oxidative stress and imbalance between the cell overall oxidants and antioxidants.

Cladosporium sphaerospermum is an environmentally-common air-borne filamentous fungus [18], and also represents a cosmopolitan species that is frequently isolated as a wide-spear of

the genus *Cladosporium* [19-21]. *Cladosporium* sp. can be isolated from air, soil, paints, plants and food materials, and these fungi have been found associated with fish diseases [22]. The implication of these fungi in human diseases was demonstrated by their isolation from superficial and intra-bronquial infections [23], and they have a documented role in causing skin lesions [23], corneal ulcers [24,25] and phaeohyphomycosis [26].

Recently, we prepared a number of pyridine-2-carboxaldehyde thiosemicarbazone ligands and investigated the structural and antimicrobial activities of their complexes with Mn(II), Ni(II), Cu(II), Zn(II) and Cd(II) ions [7, 27-31]. In this work, we have investigated the reaction of two of the ligands (**Figure 1**), **HL^1** [4-(4-nitrophenyl)-1-((pyridin-2-yl)methylene)thiosemicarbazide] and **HL^2** [4-(2-chloro)-1-((pyridin-2-yl)methylene)thiosemicarbazide] with the heavy metal ions Pb(II) and Hg(II). We have further investigated the ability of the resulting metal complexes to inhibit growth of the human pathogen *Cladosporium sphaerospermum* through their effect on the cellular soluble protein, dry mass, total antioxidant and sugar consumption. Insight into the fungal defense mechanisms against heavy metal complexes was obtained by measuring the superoxide dismutase (SOD) and catalase (CAT) enzyme activities, as these enzymes are essential in maintaining cell function in the presence of reactive oxygen species generated by anti-fungal heavy metal complexes [32-35].

2. Experimental Section

2.1 Materials and Physical Methods

Syntheses were performed in ambient atmosphere with no exclusion of air. Analytical grade chemicals were purchased and were used as received. The ligands were synthesized according to the published procedures [7,36]. CHNS contents were determined using a Vario EL III elemental analyzer. ^{1}H-NMR and ^{13}C-NMR spectra in DMSO-d_6 were measured on a

Bruker 400 MHz spectrometer, whereas tetramethylsilane acts as an internal reference. Infrared spectra were measured using a Nicolet iS10 FT-IR Spectrometer (samples in KBr pellets). A Perkin - Elmer Lambda 40 UV/VIS Spectrometer was used to record the electronic spectra. Electrical conductivities of the complexes, as $1x10^{-4}$ M DMF solutions, were measured using a Jenway 4320 conductivity meter.

2.2 Syntheses

A solution of 0.5 mmol of the appropriate metal precursor [$Pb(NO_3)_2$ (166 mg), $HgCl_2$ (136 mg)] in a minimum amount of water was added to an ethanolic solution (150 mL) of the ligand (1 mmol) [**HL^1** (301 mg), **HL^2** (291 mg)] with vigorous stirring. The solutions were refluxed for 4 hours and left to cool in the room temperature. The separated solids were filtered, washed with boiling water, absolute ethanol and diethyl ether and dried in the air.

$[Pb(L^1)_2]$ **1:** Yellow, 63 % yield. Anal. Calcd. (Found) for $C_{26}H_{20}N_{10}O_4S_2Pb$ (MW = 807.83 g/mol): C, 38.66 (38.32) %; H, 2.50 (2.49) %; N, 17.34 (17.93) %; S, 7.94 (8.22) %. FT-IR (KBr, cm^{-1}): 3341 υ(^{4}NH), 1593 υ(N=C), 1522 υ(C=N), 1281-812 [υ(CS) + υ(CN)], 1078 υ(N–N), 681 Py(iP), 435 $\upsilon(Pb–N_{azomethine})$. Molar conductance (DMF, $\Omega^{-1}cm^2mol^{-1}$): 3.24. Electronic (DMF, nm): 323.

$[Pb(L^2)_2]$ **2**: Yellow, 51 % yield. Anal. Calcd. (Found) for $C_{26}H_{20}Cl_2N_8S_2Pb$ (MW = 786.71 g/mol): C, 39.69 (39.52) %; H, 2.56 (2.51) %; N, 14.24 (14.81) %; S, 8.15 (8.43) %. FT-IR (KBr, cm^{-1}): 3329 υ(^{4}NH), 1589 υ(N=C), 1520 υ(C=N), 1311-821 [υ(CS) + υ(CN)], 1107 υ(N–N), 651 Py(iP), 416 $\upsilon(Pb–N_{azomethine})$. Molar conductance (DMF, $\Omega^{-1}cm^2mol^{-1}$): 7.15. Electronic (DMF, nm): 324, 341.

$[Hg(L^1)_2]$ **3**: Yellow, 59 % yield. Anal. Calcd. (Found) for $C_{26}H_{20}N_{10}O_4S_2Hg$ (MW = 801.23 g/mol): C, 38.98 (38.51) %; H, 2.52 (2.60) %; N, 17.48 (17.11) %; S, 8.00 (8.35) %. FT-IR

(KBr, cm^{-1}): 3337 υ(^{4}NH), 1594 υ(N=C), 1522 υ(C=N), 1289-819 [υ(CS) + υ(CN)], 1090 υ(N–N), 685 Py(iP), 442 υ(Hg–$N_{azomethine}$). Molar conductance (DMF, $\Omega^{-1}cm^2mol^{-1}$): 14.23. Electronic (DMF, nm): 323.

[Hg(L^2)$_2$] **4**: Yellow, 77 % yield. Anal. Calcd. (Found) for $C_{26}H_{20}Cl_2N_8S_2Hg$ (MW = 780.12 g/mol): C, 40.03 (39.62) %; H, 2.58 (2.45) %; N, 14.36 (14.11) %; S, 8.22 (8.83) %. FT-IR (KBr, cm^{-1}): 3335 υ(^{4}NH), 1591 υ(N=C), 1520 υ(C=N), 1315-827 [υ(CS) + υ(CN)], 1093 υ(N–N), 650 Py(iP), 418 υ(Hg–$N_{azomethine}$). Molar conductance (DMF, $\Omega^{-1}cm^2mol^{-1}$): 5.03. Electronic (DMF, nm): 324, 342.

2.3 X-Ray Crystallography

Yellow X-ray-quality crystals of complexes **2** and **3** were grown by the slow cooling of hot dichloromethane (**2**) or acetonitrile (**3**) solutions of the complexes. X-ray diffraction data for both compounds were collected at 173 K using a Rigaku FR-X Ultrahigh Brilliance Microfocus RA generator/confocal optics with XtaLAB P200 diffractometer [MoKα radiation (λ = 0.71073 Å)]. Intensity data were collected using ω steps accumulating area detector images spanning at least a hemisphere of reciprocal space. Data for all compounds analysed were collected using CrystalClear [37] and processed (including correction for Lorentz, polarization and absorption) using CrysAlisPro [38]. Structures were solved by direct methods (SIR2011 [39]) and refined by full-matrix least-squares against F^2 (SHELXL-2018/3[40]).

Non-hydrogen atoms were refined anisotropically, and hydrogen atoms were refined using a riding model, except for nitrogen-bound hydrogens which were located from the difference-Fourier map and refined isotropically subject to distance restraints. All calculations were performed using the Olex2 [41] interface. Molecular graphics for the complexes were drawn using ORTEP-III [42], while the packing diagrams for the complexes (**Figure S1**) were

drawn using VESTA (Ver. 3.5.5) [43]. Selected crystallographic data are presented in **Table 1**. Deposition numbers 2127785-2127786 contains the supplementary crystallographic data for this paper. These data are provided free of charge by the joint Cambridge Crystallographic Data Centre and Fachinformationszentrum Karlsruhe Access Structures service www.ccdc.cam.ac.uk/structures.

2.4 Microorganism identification

Cladosporium sphaerospermum was isolated as air-spora of a green area around a public hospital on potato dextrose agar medium (PDA) containing (g/l): potato (scrubbed and diced), 200; dextrose, 20.0; agar, 15.0 in distilled water (pH 5.6). The medium was supplemented with rose bengal (50 mg/l) and chloramphenicol (250 µg/mL) as bacteriostatic and bactericidal agents. The climatic conditions of the isolation day were as follows: maximum temperature (26.7 °C), minimum temperature (22°C), wind speed (17.2 Km/h) and relative humidity (36%). Twenty plates filled with medium were opened for 10 minutes in different places around the hospital, and incubated aerobically at 28± 1 °C for a week prior to maintaining the isolates at 4±1 °C on PDA slant until they were tested. The morphological characters of *C. sphaerospermum* were identified according to Domsch [19] on malt agar medium (MA) containing (g/l): malt extract, 20.0; glucose, 20.0; peptone, 1.0 and agar, 15.0 in distilled water. Afterwards, the isolate was molecularly identified by SolGent, Daejeon, South Korea by using ITS 1 and 4 primers that bind to the conserved regions of the fungal 18S rRNA gene (detailed information is given in supporting information file). The sequence was analyzed by BLAST from the National Center of Biotechnology Information (NCBI) website and was deposited in GenBank database for accession numbers.

2.5 Medium and inoculums

Czapek's broth growing medium was prepared by adding (g/l): glucose, 30.0; yeast extract, 5.0; $NaNO_3$, 3.0; KH_2PO_4, 1.0; $MgSO_4 \cdot 7H_2O$, 0.5; KCl, 0.5 and $FeSO_4 \cdot 7H_2O$, 0.01 in distilled water. After autoclaving this medium at 121 ℃ and 1.5 atm. for 20 minutes, chloramphenicol (250 μg/mL) sterilized by a membrane with a pore size of 0.22 mm was added. *Cladosporium* inoculum was prepared by scraping a five day old grown culture on MA plats into sterilized distilled water containing triton X100 (0.1%, v/v) before it was diluted to 2×10^5 spore/mL [44].

2.6 Effect of complexes 1-4 on *C. sphaerospermum* growth and sugar consumption

The complexes were suspended in water at concentrations of 0, 0.1, 0.6, 1.2, 1.8 and 2.4 mM and were added to flasks containing 50 mL of Czapek's broth medium. After adding *Cladosporium* inoculums (1%, v:v), the flasks were incubated on a rotary shaker (28±1°C, 150 rpm) for a week. After incubation, *Cladosporium* biomass was filtered by using Whatman filter paper No. 113, washed with water and dried in a hot air oven at 70 ℃ until constant determination of the dry mass (DM) [45]. Fungal filtrate was collected and centrifuged at 5000 g for 10 minutes to remove any fungal residuals or spores and the supernatant was used for the residual sugar estimation. The fungal spores were also tested for their viability being one milliliter from the fungal filtrate was transferred into a sterilized Petri dish and mixed with 25 milliliters of sterilized PDA medium. After solidification, the plates were incubated aerobically at 28± 1 ℃ for a week and the colony growth was detected [45].

2.7 Effect of metal ions and free ligands on *C. sphaerospermum* growth

The effects displayed by both of the metal ions and free ligands on the fungal growth were tested at the same concentrations of 0, 0.1, 0.6, 1.2, 1.8 and 2.4 mM comparing with nystatin

as a standard antifungal agent. After incubation, *Cladosporium* biomass was filtered by using Whatman filter paper No. 113, washed with water and dried in a hot air oven at 70 °C until constant determination of the dry mass (DM) [45].

2.8 Oxidative stress generation by the complexes

Czapek's broth medium flasks containing 1% inoculum and the complexes at concentrations of 0, 0.1, 0.6, 1.2, 1.8 and 2.4 mM were incubated on a rotary shaker (150 rpm) at 28±1 °C for a week. Afterwards the biomass was filtered and washed with distilled water. *Cladosporium* mycelia were mechanically disrupted in cold mortar under liquid nitrogen conditions until complete mycelia breakage and the disrupted mycelia were extracted by using a potassium phosphate buffer solution (pH = 7.8) containing EDTA (0.1 mM) and polyvinyl pyrrolidone PVA (0.1 g). The extracts were centrifuged (18,000 rpm) for 10 minutes at 4°C before the supernatants were estimated for soluble proteins (SP), total antioxidants (TA), SOD activity and CAT activity [46].

2.9 Analytical assays

Residual sugar content was measured by using the anthrone-sulfuric acid reagent [47]; reacting the reagent (4.5 mL) with the supernatant (0.2 mL) at 100 ºC for ten minutes. After cooling, the absorbance was measured at 620 nm where the blank solution contained no free sugar and the sugar quantities were estimated from the standard curve of glucose. Soluble proteins (SP) were estimated by using the Folin reagent at 750 nm according to the standard curve of bovine serum albumin and the results were expressed in mg/g fresh weight [48]. Total antioxidant (TA) was determined (as mg/g soluble protein) by using the phosphomolybdenum method at 695 nm according to the standard curve of ascorbic acid [49]. The SOD (EC 1.15.1.1) was assayed via epinephrine (adenochrome) autoxidation according to the modified method [50] in which the SOD activity was measured at 480 nm

for 1 minute, while the CAT (1.11.1.6) activity was assayed by measuring the consumption of hydrogen peroxide for 1 minute at 240 nm [51]. All colorimetric and UV measurements were performed by using a T60 split beam UV spectrophotometer with a fixed slit of 2 nm covering the wavelength range of 190–1100 nm.

3. Results and Discussion

3.1 Synthesis and characterization

The TSC ligands **HL^1** [36] and **HL^2** [7] were synthesized by reacting substituted phenylisothiocyanates and hydrazine hydrate following by condensation with pyridine-2-carboxylaldehyde according to published procedures. The ligands were characterized according to their CHNS contents and FT-IR, UV-VIS., ^{1}H-NMR and ^{13}C-NMR spectral data. ^{1}H-NMR spectra of both ligands in DMSO-d_6 show three singlet peaks attributed to NH(hydrazine), NH(thiourea) and N=CH(azomethine) protons and these peaks appear respectively at 12.24, 10.44 and 8.58 ppm for **HL^1** and at 12.15, 10.24 and 8.18 ppm for **HL^2**. Moreover, other sets of doublets and triplets ranging from 8.36 to 7.39 ppm for **HL^1** and from 8.59 to 7.31 ppm for **HL^2** due to the pyridinyl and phenyl CH protons are found in the respective spectra. The ligands have shown usefulness in coordination chemistry with a chelation mode of pyridine-2-carboxaldehyde TSC ligands via the azomethine (N), pyridinyl (N) and thiolate (S) atoms in a monobasic character that has been shown by single crystal XRD studies of respective metal complexes [7,27-31]. These tridentate ligands are stable at room temperature and exhibit thione – thiol tautomerism in the solid form, but the thiol conformation is predominant in the ligand solution [28-31]. The reaction of Pb(II) and Hg(II) with the TSCs took place in aqueous ethanol under refluxing conditions and the solids formed were washed extensively with boiling water to remove unreacted metal precursor.

The yellow complexes were obtained in moderate yields (51-77 %) and exhibited very poor solubility at room temperature in several organic solvents, e.g. methanol, ethanol, acetone and methylene chloride. They showed sufficient solubility in DMF (10^{-4} M) for conductivities to be measured, and in all cases the formation of neutral complexes was indicated by their negligible molar conductivities (3.24-14.23 $\Omega^{-1}cm^2mol^{-1}$) [52]. The general chemical formula $[M(L)_2]$ [M = Pb(II) or Hg(II) and L = L^1 or L^2] was assigned for all four metal complexes from their CHNS analyses in the solid state, and an octahedral geometry around the metal centers was suspected considering the tridentate monobasic nature of the ligands and the formula of the complexes. Refluxing the complexes in dichloromethane (**2**) or acetonitrile (**3**) led to their dissolution and, upon cooling the solutions in air, formation of X-ray quality crystals of these two complexes. Of which, single crystals of complexes **2** and **3** were in sufficient quality for XRD studies. Crystals of complex **2** (0.01x0.02x0.13 mm) and complex **3** (0.02x0.04x0.08 mm) were analyzed. **Figures 2** and **3** display the molecular structures of complexes **2** and **3**. Selected crystallographic data are presented in **Table 1**, and selected bond distances and bond angles are depicted in **Tables 2** and **S1**.

Both complexes crystallized in the triclinic space group $P\overline{1}$, although adopting different unit cells. They show the expected octahedral geometry around the metal, the anionic ligands coordinating via the pyridine N (N1, N18), azomethine N (N8, N25) and thiol S (S10, S27) atoms. This coordination mode leads to the formation of four 5-membered metallacycles in each complex. The structures of the two complexes, as expected, are similar, with two primary differences arising. The first is differences in the degree of planarity of some of the ligands. In complex **2** both ligands adopt a planar arrangement (mean deviations from plane 0.056 and 0.137 Å), aided by the ability of these ligands to form stabilizing intramolecular N–H···Cl hydrogen bonds (**Table S2**), while in complex **3**, where such classic intramolecular hydrogen bonds are not possible, one ligand shows greater deviation from planarity (mean

deviations from plane 0.078 and 0.260 Å). The second is the differing relative orientation of the two ligands in each complex, the ligands in complex **3** being oriented closer to orthogonal to each other (**2**: 76.5°, **3**: 88.7°), leading to it adopting a geometry closer to a regular octahedron.

UV-VIS. and FT-IR spectra of all ligands and complexes were measured. UV-VIS. spectroscopic data were measured in DMF solutions, and only a single peak at 333 nm for $\mathbf{HL^1}$ and two peaks at 322 and 338 nm for $\mathbf{HL^2}$ were recorded. However complexes **1-4** suffered insignificant shift of 2-4 nm in the spectra comparing to the ligands. The significant FT-IR vibrational bands of $\mathbf{HL^1}$, $\mathbf{HL^2}$ and complexes **1-4** were identified. The contribution of the TSC N(4)H atoms in forming hydrogen bonds, both intra- and intermolecular, result in a shift in the N–H stretching frequency in the spectra of complexes **1-4** to higher values (3329 – 3341 cm^{-1} in the complexes, in comparison to 3304 and 3268 cm^{-1} for $\mathbf{HL^1}$ and $\mathbf{HL^2}$, respectively [7]). The other υ(NH) band of the TSC ligand that appear at 3116 cm^{-1} in the spectrum of $\mathbf{HL^1}$ and 3130 cm^{-1} in the spectrum of $\mathbf{HL^2}$ is absent in the spectra of complexes **1-4** and this indicates the coordination of $\mathbf{HL^1}$ and $\mathbf{HL^2}$ in their deprotonated thiol form [27]. The thiol(S) coordination in the complexes could also be proved by the movement of the two thioamide bands [υ(CS) + υ(CN)] (1330 and 846 cm^{-1} in $\mathbf{HL^1}$, 1320 and 868 cm^{-1} in $\mathbf{HL^2}$) to lower wavenumbers in the spectra of complexes **1-4** [28]. There are also bands due to υ(C=N) (1591 cm^{-1} in $\mathbf{HL^1}$, 1586 cm^{-1} in $\mathbf{HL^2}$) which shift to a range of 1520-1522 cm^{-1} in the spectra of the complexes, confirming coordination of the azomethine moiety [29]. Coordination of the N(pyridine) atoms can also be investigated by positive shifts regarding the in-plane ring deformation bands found in the IR spectra of the ligands at 664 for $\mathbf{HL^1}$ and 621 cm^{-1} for $\mathbf{HL^2}$ [31].

3.2 Identification of *Cladosporium sphaerospermum* ASU18 (MK387875)

The morphology of *Cladosporium sphaerospermum* (Penzig) (**Figure 4**) was described by Domsch et. al. [19] as slowly growing colonies (dark olive green) with black reverse on malt extract agar medium (MEA). Conidiophore erects almost smoothly with no swellings up to length of 300 μm and thickness of 3-5 μm in addition to several acropleurogenous conidial chains. Conidia are mostly olive brown globose or sub-globose and ramo-conidia usually elongate with 8.5-13.5 μm long × 3-3.5 μm diameter [19]. The isolate was identified as *Cladosporium sphaerospermum* (ASU18) MK387875 by analyzing the 18S rRNA gene sequence. The sequence of 513 base pairs was similar with 99 % to *Cladosporium sphaerospermum* KU064688, with 99 % to *Cladosporium sphaerospermum* KX034375 and with 99% to *Cladosporium sphaerospermum* KJ173531. Sandoval-Denis et. al. [53] analyzed and distinguished between ninety-two *Cladosporium* clinical isolates by phenotypic and molecular methods, and utilized ITS sequence analysis and D1/D2 regions in United States.

3.3 Effect of complexes 1-4 on *C. sphaerospermum* growth and sugar consumption

The effect of complexes **1-4**, in the concentration range of 0.1-2.4 mM, on the growth and sugar consumption of *C. sphaerospermum* is shown in **Figure 5**. Increasing the concentration of complexes **1-4** suppressed the fungal growth, and interestingly complexes **2** and **4** inhibited the fungal growth completely at concentrations greater than 1.8 mM. For fungal samples treated with the complexes, biomasses of 2.13-5.59, 0.0-3.03, 1.47-5.49 and 0-1.6 g/l were found for complexes **1-4**, respectively, while the control samples contained fungal biomass of 6.45±0.18 g/l. The level of sugar consumption by the fungus in the presence of complexes **1-4** also decreased as the concentration of the complexes increased. Further, we found that the generated spores of *C. sphaerospermum* after treating with the complexes are still viable and can undergo regrowth in PDA medium. Nevertheless, the fungal total counts

decreased compared to the control (untreated) sample (**Figure S2**). Sugar consumption of 70.2 % was recorded for the control samples, while the consumed sugar percentages were 28.9-56.9, 0.0-49.80, 21.3-58.3 and 0.0-21.5 % in the presence of varying levels of complexes **1-4**, respectively.

Both of these metrics indicate that for the same TSC ligand that the Hg(II) complexes lead to enhanced fungal growth inhibition compared to Pb(II) ones, and also that complexes containing $\mathbf{HL^2}$ inhibit fungal growth more than those containing $\mathbf{HL^1}$. The latter point may arise from the slightly higher nitrogen content in the complexes based on $\mathbf{HL^1}$, as nitrogen is an essential element for fungal growth and it is known that lower nitrogen content can lead to greater inhibition of fungal growth [54]. In literature, it is documented tolerance between the fungal biomass and concentration of heavy metals [55], despite documenting fungal growth even at high heavy metal concentrations via cell wall metal-binding characteristics [56,57]. However, in this paper, complex **1-4** that contain Pb(II) and Hg(II) as heavy metal tolerants and absorbers [58,59] were able to completely inhibit the *Cladosporium* growth.

3.4 Effect of complexes 1-4 on *C. sphaerospermum* antioxidant system

The effect of complexes **1-4**, in the concentration range of 0.1-2.4 mM, on the intracellular total antioxidants (TA), soluble proteins and SOD and CAT enzymes of *C. sphaerospermum* was also investigated (**Figure 6**). Total antioxidant values reflect the metabolic stress picture inside the fungal cells. Increasing the concentration of complexes **1-4**, respectively, raised the total antioxidant (enzymatic and non-enzymatic) content to maximum values of 10.07, 5.73, 10.37 and 5.46 mg/g protein in comparison to the value of 3.44 mg/g protein recorded for the control sample. However, the total antioxidants started to diminish at concentrations above 1.2 mM for complexes **1** and **3** and at above 0.6 mM for complexes **2** and **4**. Soluble proteins were also estimated and the control sample was found to contain soluble proteins of 4.34

mg/g fresh weight. However, in the cultures containing complexes **1**-**4**, soluble proteins in the ranges of 1.95-4.37, 0.0-3.16, 3.0-3.97 and 0.0-6.22 mg/g fresh weight, respectively, were determined.

One of the effects of metal-containing complexes on cells can be the production of ROS, causing oxidative stress. This disturbance to the cellular redox conditions can lead to enhanced expression of antioxidant enzymes to remove these ROS [60]. SOD enzymes catalyze the dismutation process of superoxide radicals into molecular dioxygen and hydrogen peroxide (H_2O_2) [34], while CAT enzymes regulate the intracellular hydrogen peroxide levels [32] by converting it into dioxygen and water [33]. Cultures containing complexes **1**-**4** (1.2 mM) displayed, respectively, maximum SOD specific activities of 2.67, 2.41, 1.88 and 0.76 in comparison to a specific activity of 0.67 determined for the control sample. Likewise, CAT enzyme specific activity increased in response to complexes **1**-**4** in comparison to the control. Specific activities of 0.45-0.81, 0.0-0.75, 0.26-0.81 and 0-0.47 were found in the fungal cultures continuing complexes **1**-**4**, respectively, while the control sample showed a specific activity of 0.05. The activities of the fungal SOD and CAT enzymes followed the trend of maximum activity at moderate concentrations of complex. Malar et. al. [34] has attributed the reduction in the cellular SOD enzyme activity at high heavy metal concentration to the production of excessive amount of hydrogen peroxide, while accumulation of H_2O_2 inside the fungal cells induces the formation of non-enzymatic antioxidants involved in the cell defense system [35] resulting in reduction in CAT activity. Huang et. al. reported that addition of lead concentrations (>100 ppm) to *Phanerochaete chrysosporium* increased SOD and CAT activities to maximum values, while higher concentrations decreased the SOD and CAT activities [61]. On the other hand, lead cations of 100 ppm enhanced and promoted the fungal *Pseudomonas putida* KNU8 antioxidant enzymes [62].

3.5 Effect of metal ions and free ligands on *C. sphaerospermum* growth

To clarify which part in the complex (the metal ion vs. the organic ligand) causes the antifungal activity, we determined the fungus dry mass under the effect of concentrations of 0.1-2.4 mM of the metal ions and free ligands comparing with nystatin as a standard antifungal agent (**Figure 7**). Clearly, mercuric chloride (10 mM) showed *C. sphaerospermum* dry mass of 4.85±0.16 g/l, while increasing its concentration to 2.4 mM produced zero dry mass (complete fungal growth inhibition). Further, the *C. sphaerospermum* dry mass upon the addition of lead nitrate decreased from 4.89±0.09 g/l to 1.34±0.11 g/l by gradual increment of lead nitrate concentration from 10 mM to 2.4 mM. On the other hand, the free ligands have only shown weak effects on the fungal growth as the fungal dry masses of 6.26±0.18 g/l and 6.2±0.13 g/l (using 10 mM of $\mathbf{HL^1}$ and $\mathbf{HL^2}$, respectively) and dry masses of 5.16±0.06 g/l and 4.56±0.07 g/l (using 2.4 mM of $\mathbf{HL^1}$ and $\mathbf{HL^2}$, respectively) were detected. Based on these results, we detected complete fungal inhibition at 1.8 mM of complexes **2** and **4**, while $HgCl_2$, $Pb(NO_3)_2$ and $\mathbf{HL^2}$ each at 1.8 mM provided dry masses of 0.88±0.18, 1.78±0.14 and 4.88±0.06 g/l, respectively. Therefore, we could assign complexes **2** and **4** as more potent inhibitors for *C. sphaerospermum* compared to the respective ligand and metals. In literature, the metal {Cu, Cd, Mn, Pb, Hg, and Zn} cations were shown to negatively impact several fungal cellular life processes resulting in their growth suppression and death [63]. Metal ions have also shown creation of precipitates or complexes with microbial metabolites causing disruption in the microbial cell membranes [64]. Specifically, cations of mercury and lead disrupt microbial cell membranes, impede enzyme performance, denature proteins and reduce fungal growth [65,66]. The caused stress in several fungal species results in a dramatic generation of reactive oxygen species (for instance, the superoxide, peroxide and hydroxyl radicals). This oxidative stress, in turn, can be regarded as

the primary cause of heavy metal-induced cell death in microorganisms, as it harms fungal cells, organelle structure and metabolism [67].

In this experiment, we included nystatin as a *Streptomyces noursei* derived polyene antifungal agent [68,69] with documented broad spectrum of activity against a variety of fungal species, e.g. *Aspergillus fumigatus, Candida albicans, Cladosporium sphaerospermum, Coccidioides immitis* and *Cryptococcus neoformans* [70-72]. This experiment indicated high activity of nystatin against *C. sphaerospermum* ASU18 (MK387875) with growth inhibition exceeding 50 % caused by 2.4 mM of nystatin. This agrees with previous results revealed the antifungal activity of nystatin against both filamentous and unicellular fungi with MIC of 2-6 µg/ml against both *A. flavus* and *A. fumigatus* and of 1-2 µg/ml against *C. albicans* [70]. Further, nystatin has also demonstrated high antifungal activity against filamentous fungi (e.g. nystatin MIC values of 1.56 µg/ml against *Penicillium granulatum*, 6.25 µg/ml against *Cladosporium carrionii, Aspergillus fumigatus* and *Aspergillus flavus* and 12.5 µg/ml against *Trichophyton violaceum* and *Mucor mucedo* were detected) [71]. This is in addition to great activity shown by nystatin against *Cladosporium sphaerospermum* and *Cladosporium cladosporioides* [73].

4. Conclusion

This work describes the complexation of the toxic heavy metals Pb(II) and Hg(II) with thiosemicarbazone ligands leading to the formation of four octahedral TSC complexes. The complexes, in appropriate and low concentrations, exhibited extreme antifungal activity against a common airborne pathogen *Cladosporium sphaerospermum* ASU18 (MK387875). The complexes were seen to influence the fungal sugar consumption, soluble proteins and total antioxidants. The complexes caused oxidative stress to the cells, resulting in enhanced expression of CAT and SOD enzymes. In general, these coordination compounds could

represent potential antifungal agents as alternatives to those that suffer from microbial resistance.

Acknowledgements

This research did not receive any specific grant from funding agencies in the public, commercial, or not-for-profit sectors.

References

[1] P.F. Rapheal, E. Manoj, M.R.P. Kurup, *Polyhedron* **2007**, 26, 5088.

[2] A.E. Liberta, D.X. West, *Biometals* **1992**, 5, 121.

[3] Z. Iakovidou, E. Mioglou, D. Mourelatos, A. Kotsis, M.A. Demertzis, A. Papagoergiou, J.R. Miller, D. Kovala-Demertzi, *Anticancer Drugs* **2001**, 12, 65.

[4] D. Kovala-Demertzi, M.A. Demertzis, J.R. Miller, C. Papadopoulou, C. Dodorou, G. Filousis, *J. Inorg. Biochem.* **2001**, 86, 555.

[5] A. Sîrbu, O. Palamarciuc, M.V. Babak, J.M. Lim, K. Ohui, E.A. Enyedy, S. Shova, D. Darvasiová, P. Rapta, W.H. Ang, V.B. Arion, *Dalton Trans.* **2017**, 46, 3833.

[6] R. Ouyang, Y. Yang, X. Tong, K. Feng, Y. Yang, H. Tao, X. Zhang, T. Zong, P. Cao, F. Xiong, N. Guo, Y. Li, Y. Miao, S. Zhou, *J. Inorg. Biochem.* **2017**, 168, 18.

[7] A.B.M. Ibrahim, M.K. Farh, S.A. El-Gyar, M.A. EL-Gahami, D.M. Fouad, F. Silva, I.C. Santos, A. Paulo, *Inorg. Chem. Commun.* **2018**, 96, 194.

[8] A.P. King, H.A. Gellineau, S.N. MacMillan, J.J. Wilson, *Dalton Trans.* **2019**, 48, 5987.

[9] H. Jeong, Y. Kang, J. Kim, B.-K. Kim, S. Hong, *RSC Adv.* **2019**, 9, 9049.

[10] K.G. Sangeetha, K.K. Aravindakshan, *Inorg. Chim. Acta* **2018**, 469, 25.

[11] G.L. Parrilha, R.P. Dias, W.R. Rocha, I.C. Mendes, D.Benetez, J. Varela, H. Cerecetto, M. Gonzalez, C.M.L. Melo, J.K.A.L. Neves, V.R.A. Pereira, H. Beraldo, *Polyhedron* **2012**, 31, 614.

[12] M. Patra, N. Bhowmik, B. Bandopadhyay, A. Sharma, *Environ. Exp. Bot.* **2004**, 52, 199.

[13] M. Fomina, K. Ritz, G.M. Gadd, *Mycol. Res.* **2003**, 107, 861.

[14] A. Hassen, N. Saidi, M. Cherif, A. Boudabous, *Bioresour. Technol.* **1998**, 64, 7.

[15] S. Wang, Q. Lv, Y. Yang, L.-H. Guo, B. Wan, X. Ren, H. Zhang, *Biochem. Pharmacol.* **2016**, 118, 109.

[16] E. Nieboer, D.H.S. Richardson, *Environ. Pollut.* **1980**, 1, 3.

[17] S.J.S. Flora, M. Mittal, A. Mehta. *Indian J. Med. Res.* **2008**, 128, 501.

[18] S. Tasic, N.M. Tasić, *Acta Fac. Med. Naiss*. **2007**, 24(1), 15.

[19] K.H. Domsch, W. Gams, T.H. Anderson, Compendium of soil fungi. Vol. 1 & 11. Academic Press, London, **1980**.

[20] P. Zalar, G.S. de Hoog, H.-J. Schroers, P.W. Crous, J.Z. Groenewald, N. Gunde-Cimerman, *Stud. Mycol.* **2007**, 58, 157.

[21] K. Schubert, J.Z. Groenewald, U. Braun, J. Dijksterhuis, M. Starink, C.F. Hill, P. Zalar, G.S. de Hoog, P.W. Crous, *Stud. Mycol.* **2007**, 58, 105.

[22] H. Bocklisch, B. Otto, *Mycoses* **2000**, 43, 76.

[23] S. Yano, K. Koyabashi, K. Kato, *Mycoses* **2003**, 46, 348.

[24] G. Badillet, C. de Blevre, S. Spizajzen, *Bull. Soc. Fr. Mycol. Med.* **1982**, 11, 69.

[25] P.K. Shuka, Z.A. Khan, B. Lal, P.K. Agrawal, O.P. Srivastava, *Sabouraudia* **1983**, 21, 137.

[26] M.R. Vieira, A. Milheiro, F.A. Pacheco, *Med. Mycol*. **2001**, 39, 135.

[27] A.B.M. Ibrahim, M.K. Farh, P. Mayer, *Inorg. Chem. Commun.* **2018**, 94, 127.

[28] A.B.M Ibrahim, M.K. Farh, J.R. Plaisier, E.M Shalaby, *Future Med. Chem.* **2018**, 10(21), 2507.

[29] A.B.M. Ibrahim, M.K. Farh, P. Mayer, *Appl. Organometal. Chem.* **2019**, 33(7), e4883.

[30] A.B.M. Ibrahim, M.K. Farh, I.C. Santos, A. Paulo, *Appl. Organometal. Chem.* **2019**, 33(9), e5088.

[31] G.A.-E. Mahmoud, A.B.M. Ibrahim, P. Mayer, *J. Biol. Inorg. Chem.* **2020**, 25, 797.

[32] O.B. Blokhina, E. Virolainen, K.V. Fagerstedt, *Ann. Bot.* **2003**, 91, 1179.

[33] F. Estruch, *FEMS Microbiology. Rev.* **2000**, 24(4), 469.

[34] S. Malar, S.S. Vikram, P.J.C. Favas, V. Perumal, *Bot. Studies* **2014**, 55, 54.

[35] P.S. Basha, A.U. Rani, *Ecotoxicol. Environ. Saf.* **2003**, 56, 218**.**

[36] V.F.S. Pape, S. Tóth, A. Füred, K. Szebényi, A. Lovrics, P. Szabó, M. Wiese, G. Szakács, *Eur. J. Med. Chem.* **2016**, 117, 335.

[37] *CrystalClear-SM Exper*t v2.1 (**2015**). Rigaku Americas, The Woodlands, Texas, USA, and Rigaku Corporation, Tokyo, Japan.

[38] *CrysAlisPro* v1.171.41.93a (**2020**). Rigaku Oxford Diffraction, Rigaku Corporation, Oxford, U.K.

[39] M.C. Burla, R. Caliandro, M. Camalli, B. Carrozzini, G.L. Cascarano, C. Giacovazzo, M. Mallamo, A. Mazzone, G. Polidori, R. Spagna, *J. Appl. Crystallogr.* **2012**, *45*, 357.

[40] G.M. Sheldrick, *Acta Crystallogr. C*. **2015**, *71*, 3.

[41] O.V Dolomanov, L.J. Bourhis, R.J. Gildea, J.A.K. Howard, H. Puschmann, *J. Appl. Crystallogr*. **2009**, *42*, 339.

[42] M.N. Burnett, C.K. Johnson, ORTEP-III: Oak Ridge Thermal Ellipsoid Plot Program for Crystal Structure Illustrations (**1996**), Oak Ridge National Laboratory Report ORNL-6895.

[43] K. Momma, F. Izumi, *J. Appl. Crystallogr.* **2011**, 44, 1272.

[44] G.A. Mahmoud, A.S.A. Zidan, A.A.M. Aly, H.K. Mosbah, A.B.M. Ibrahim, *Appl. Organometal. Chem.* **2018**, 33(2), e4740.

[45] H. N. Abdelhamid, G. A-E. Mahmoud, W. Sharmouk. *J. Mater. Chem. B.* **2020**, 8, 7548.

[46] A.B.M. Ibrahim, G. A-E. Mahmoud, *Appl Organomet Chem.* **2021,** 35(2), e6086.

[47] E.W. Yemm, A.J. Willis, *New Phytol.* **1994**, 55, 229.

[48] O.H. Lowry, N.J. Rosebrough, A.L. Farr, R.J. Randall, *J. Biol. Chem.* **1951**, 193, 265.

[49] P. Prieto, M. Pineda, M. Aguilar, *Anal. Biochem.* **1999**, 269, 337.

[50] H.P. Misra, I. Fridovich, *J. Biol. Chem.* **1972**, 247, 3170.

[51] T. Matsumura, N. Tabayashi, Y. Kamagata, C. Souma, H. Saruyama, *Physiol. Plant.* **2002**, 116, 317.

[52] W.J. Geary, *Coord. Chem. Rev.* **1971**, 7, 81.

[53] M. Sandoval-Denis, D.A. Sutton, A. Martin-Vicente, J.F. Cano-Lira, N. Wiederhold, J. Guarro, J. Gené, *J. Clin. Microbiol.* **2015**, 53, 2990.

[54] A. Pfannmüller, J.M. Boysen, B. Tudzynski, *Front. Microbiol.* **2017**, 8, 381.

[55] P. Baldrian, *Enzym. Microb. Technol.* **2003**, 32, 78.

[56] P. Anand, J. Isar, S. Saran, R.K Saxena, *Bioresour. Technol.* **2006**, 97, 1018.

[57] R. Gupta, P. Ahuja, S. Khan, R.K. Saxena, H. Mohapatra, *Curr. Sci.* **2000**, 78(8), 967.

[58] D. Xinjiao, *J. Environ. Biol.* **2006**, 27, 639.

[59] M.C. Romero, E.H. Reinoso, M.I. Urrutia, A.M. Kiernan, *J. Biotechnol.* **2006**, 9, 222.

[60] A. Halienova, I. Marova, M. Carnecka, H. Konecna, V. Hanusova, V. Hezinova, *J. Biotechnol.* **2007**, 131(2), S202.

[61] H. Chao, C. Lai, P. Xu, G. Zeng, D. Huang, J. Zhang, C. Zhang, M. Cheng, J. Wan, R. Wang, *Chemosphere* **2017**, 187, 70.

[62] K.A. Hussein, J.H. Joo, *Afr. J. Microbiol. Res.* **2013**, 7(20), 2288.

[63] A. Bano, J. Hussain, A. Akbar, K. Mehmood, M. Anwar, M.S. Hasni, S. Ullah, S. Sajid, I. Ali, *Chemosphere* **2018**, 199, 218.

[64] D. Sobolev, M.F.T. Begonia, *Int. J. Environ. Res. Public Health* **2008**, 5, 450.

[65] M. Graz, B. Pawlikowska-Pawlega, A. Jarosz-Wilkolazka, *Int. Biodeterior. Biodegrad.* **2011**, 65, 124.

[66] A.S. Yangbenro, O.O. Babalola, *Int. J. Environ. Res. Public Health* **2017**, 14, 94.

[67] Y. Lin, W. Xiao, Y. Ye, C. Wu, Y. Hu, H. Shi, *Environ. Sci. Pollut. Res.* **2020,** 27, 27819.

[68] E.L. Hazen, R. Brown, *Proc. Soc. Exp. Biol. Med.* **1951**, 76, 93.

[69] V. C. Stanley, M.P. English. *J. Gen. Microbiol.* **1965**, 40, 107.

[70] M. Schaefer-Korting, J. Blechschmidt, H.C. Korting, *Mycoses* **1996**, 39, 329.

[71] E.M. JOHNSON, J.O. Ojwang, A. Szekely, T.L. Wallace, D.W. Warnock *Antimicrob. Agents Chemother.* **1998**, 42, 1412.

[72] V.V. Belakhov, Y.D. Shenin, *Pharm. Chem. J.* **2008**, 42, 15.

[73] A.A. Morandim, A.R. Pin, N.A.S. Pietro, A.C. Alecio, M.J. Kato, C.M. Young, J.E. de Oliveira, M. Furlan, *Afr. J. Biotechnol.* **2010**, 9, 6135.

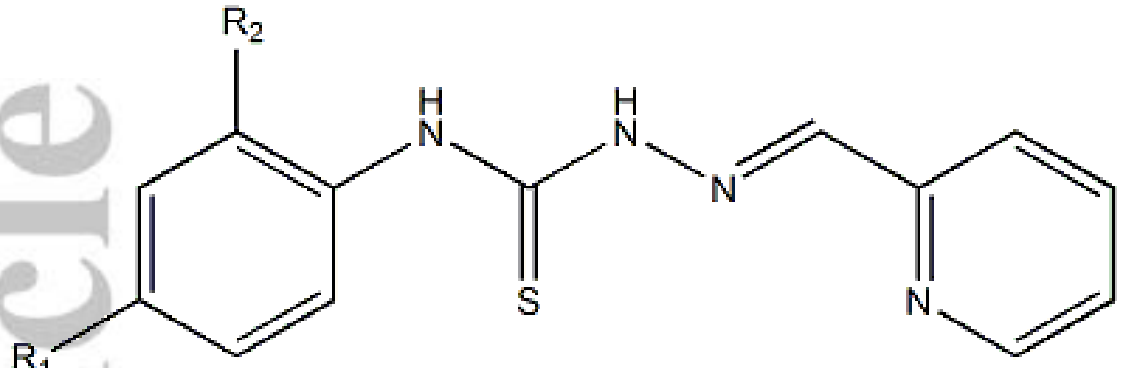

$R_1 = NO_2$ and $R_2 = H$ **HL**^{1}

$R_1 = H$ and $R_2 = Cl$ **HL**^{2}

FIGURE 1 Molecular structures of the ligands

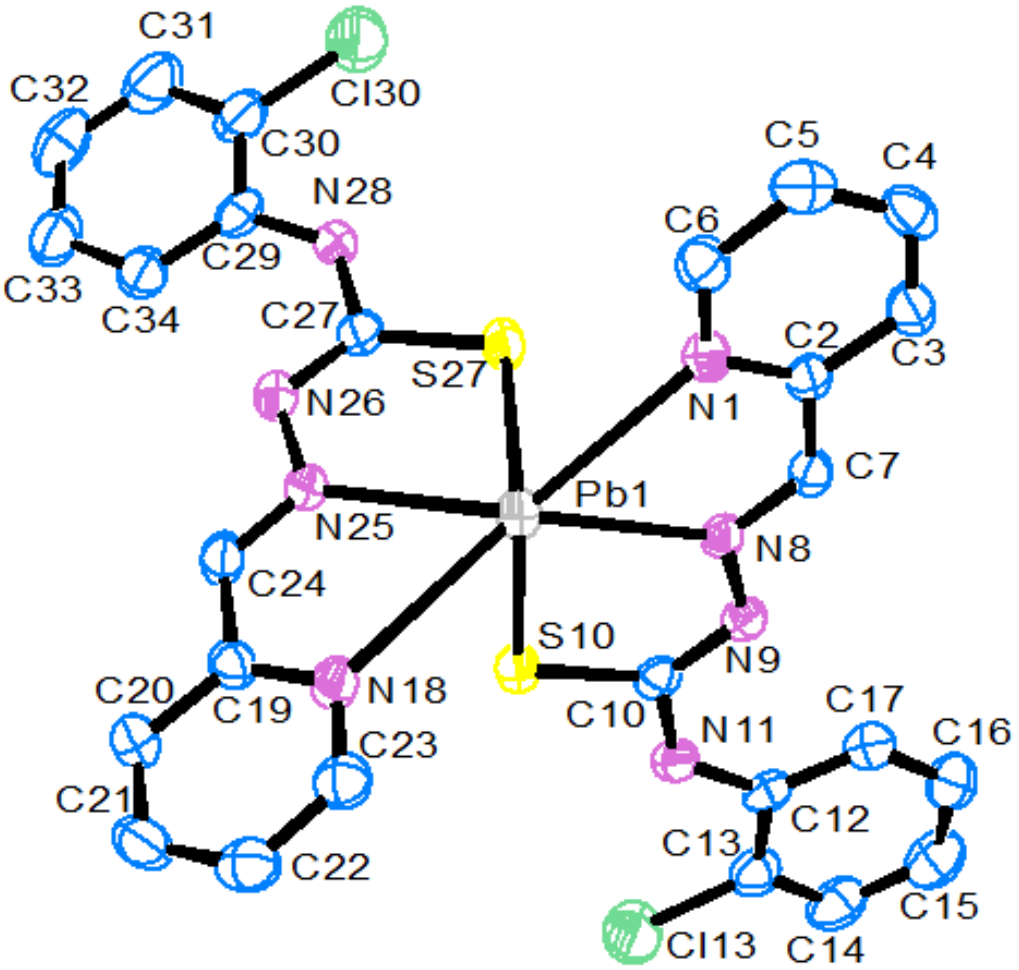

FIGURE 2 ORTEP diagram with atom numbering scheme of complex **2**. Thermal displacement ellipsoids are drawn at the 50 % probability level

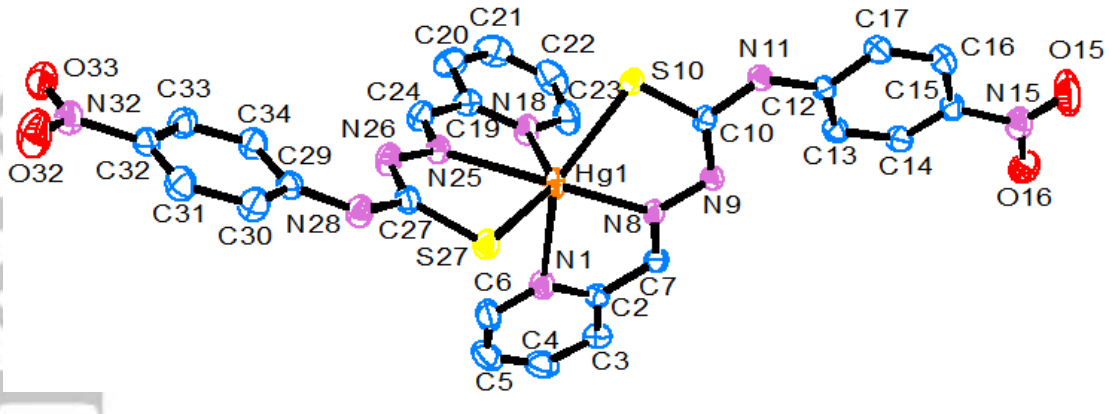

FIGURE 3 ORTEP diagram with atom numbering scheme of complex **3**. Thermal displacement ellipsoids are drawn at the 50 % probability level.

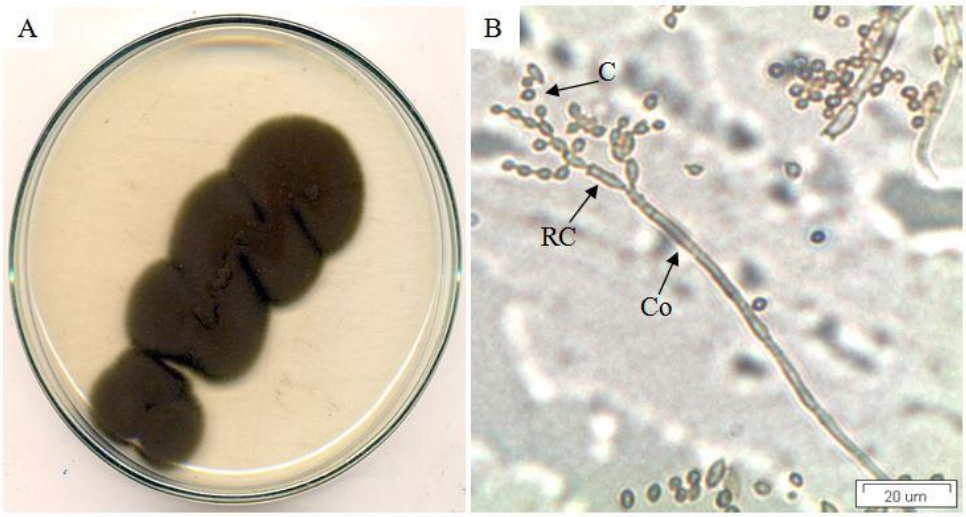

FIGURE 4 *Cladosporium sphaerospermum* Penzig, A: dark olive green growth on ME agar medium; B: Microscopic feature including conidiophore (Co); ovate conidia (C) and ramo-conidia (RC); Bars, 20 µm

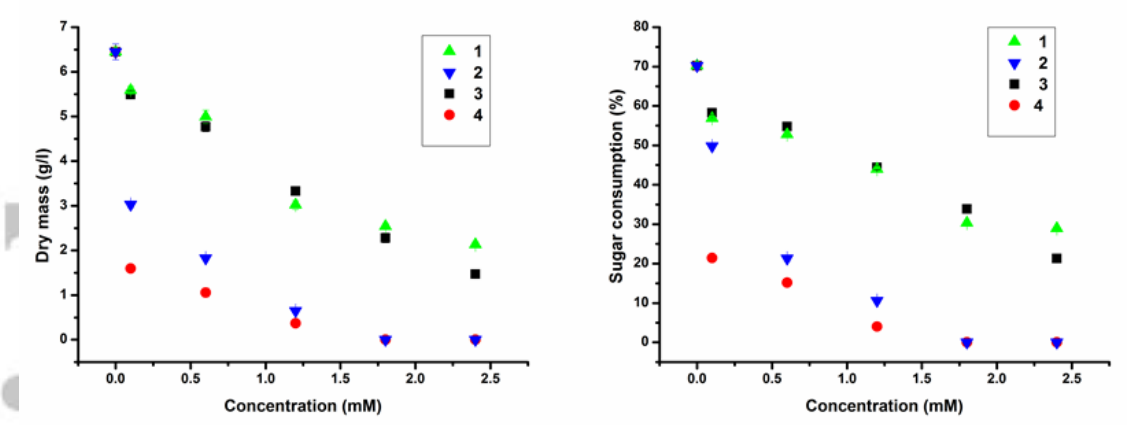

FIGURE 5 Effect of complexes **1-4** on *Cladosporium sphaerospermum* ASU 18 (MK387875) dry mass (g/l, left) and sugar consumption (%, right)

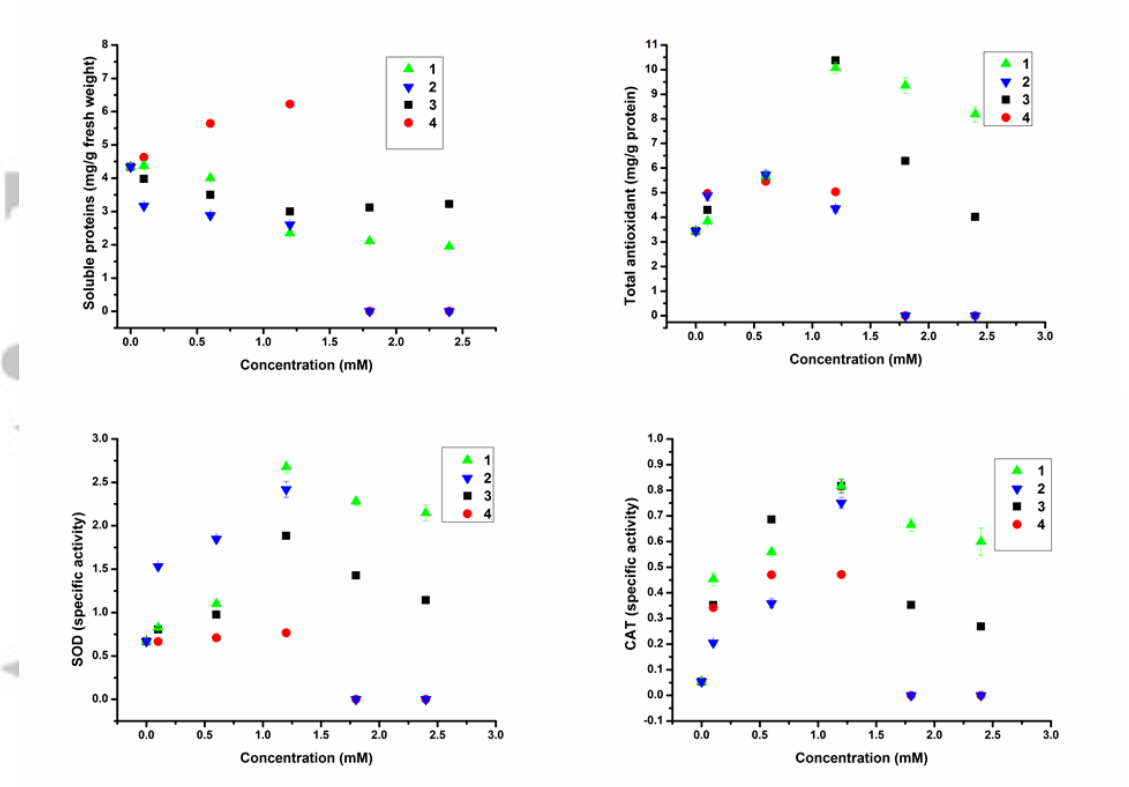

FIGURE 6 Effect of complexes **1-4** on *Cladosporium sphaerospermum* ASU 18 (MK387875) soluble proteins (top left), total antioxidant (top right), superoxide dismutase enzyme (bottom left) and catalase enzyme (bottom right)

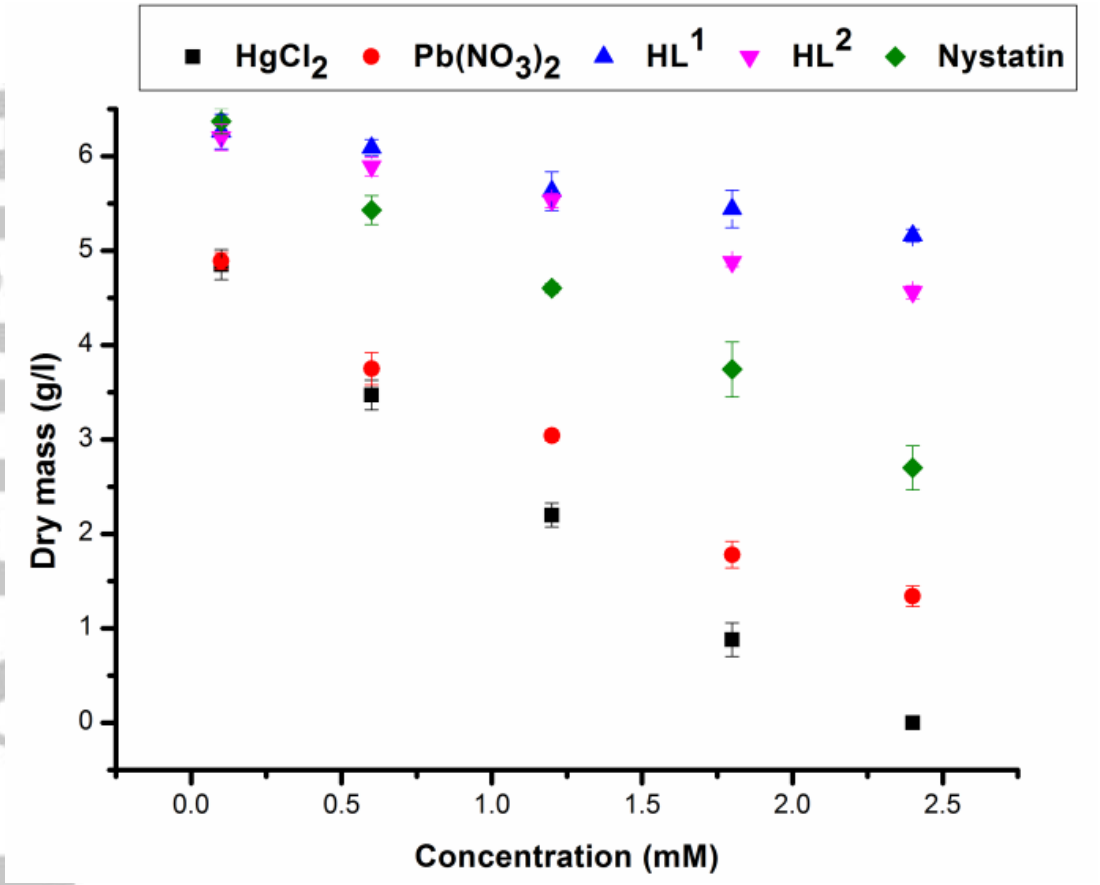

FIGURE 7 Effect of metal ions, free ligands and nystatin (a standard antifungal agent) on *C. sphaerospermum* ASU 18 (MK387875) dry mass (g/l).

TABLE 1 Crystallographic data for complexes **2** and **3**

	2	**3**
CCDC Reference Number	2127785	2127786
Empirical formula	$C_{26}H_{20}Cl_2N_8S_2Pb$	$C_{26}H_{20}N_{10}O_4S_2Hg$
Formula weight	786.71	801.23
Crystal description	Yellow needle	Yellow prism
Crystal size [mm^3]	0.13×0.02×0.01	0.08×0.04×0.02
Space group	$P\bar{1}$	$P\bar{1}$
a [Å]	6.82388(17)	8.57511(12)
b [Å]	14.4615(4)	12.12878(15)
c [Å]	14.5167(4)	14.2126(2)
α [°]	97.058(2)	98.7970(11)
β [°]	97.361(2)	94.3350(12)
γ [°]	91.786(2)	104.2638(12)
Volume [$Å^3$]	1408.39(6)	1405.83(4)
Z	2	2
Calculated density [g/cm^{-3}]	1.855	1.893
μ mm^{-1}	6.360	5.677
F(000)	760	780
Reflections collected	36780	24747
Independent reflections (R_{int})	6601 (0.0551)	6378 (0.0185)
Parameters, restraints	360, 2	396, 2
R_1 [$I > 2\sigma(I)$]	0.0316	0.0196
wR_2 (all data)	0.0628	0.0460
GoF on F^2	1.002	1.048
Largest diff. peak , hole [e $Å^{-3}$]	1.447/-1.248	1.860/-0.410

TABLE 2 Selected bond distances and bond angles in complexes **2** and **3**

Atoms	Distances (Å)	Atoms	Angles (°)	Atoms	Angles (°)
Complex 2					
Pb1—S10	2.717(1)	S10—Pb1—S27	90.61(3)	S27—Pb1—N25	68.01(7)
Pb1—S27	2.704(1)	S10—Pb1—N1	128.64(6)	N1—Pb1—N8	60.87(8)
Pb1—N1	2.845(3)	S10—Pb1—N8	68.10(7)	N1—Pb1—N18	148.43(8)
Pb1—N8	2.633(3)	S10—Pb1—N18	75.54(6)	N1—Pb1—N25	135.27(9)
Pb1—N18	2.898(3)	S10—Pb1—N25	79.93(7)	N8—Pb1—N18	133.40(9)
Pb1—N25	2.640(3)	S27—Pb1—N1	77.10(6)	N8—Pb1—N25	135.29(9)
		S27—Pb1—N8	81.52(7)	N18—Pb1—N25	60.18(9)
		S27—Pb1—N18	127.85(7)	Pb1—S10—C10	102.9(1)
Complex 3					
Hg1—S10	2.5308(7)	S10—Hg1—S27	126.58(2)	S27—Hg1—N25	74.72(5)
Hg1—S27	2.4879(6)	S10—Hg1—N1	138.66(5)	N1—Hg1—N8	66.49(6)
Hg1—N1	2.611(2)	S10—Hg1—N8	74.87(5)	N1—Hg1—N18	76.03(6)
Hg1—N8	2.361(2)	S10—Hg1—N18	84.82(5)	N1—Hg1—N25	92.30(6)
Hg1—N18	2.734(2)	S10—Hg1—N25	111.63(5)	N8—Hg1—N18	81.95(7)
Hg1—N25	2.437(2)	S27—Hg1—N1	91.27(5)	N8—Hg1—N25	143.60(6)
		S27—Hg1—N8	131.78(5)	N18—Hg1—N25	63.78(6)
		S27—Hg1—N18	135.63(5)	Hg1—S10—C10	97.92(8)

New theiosemicarbazone complexes with Pb(II) and Hg(II) ions were isolated and structurally characterized. The complexes affected the antioxidant system of *Cladosporium sphaerospermum* leading to a reduction in the fungal dry mass and sugar consumption, and varied values of the fungal total antioxidants, soluble proteins, and SOD and CAT activities.